We are IntechOpen,
the world's leading publisher of
Open Access books
Built by scientists, for scientists

7,000
Open access books available

187,000
International authors and editors

205M
Downloads

154
Countries delivered to

Our authors are among the

TOP 1%
most cited scientists

12.2%
Contributors from top 500 universities

BOOK CITATION INDEX CLARIVATE ANALYTICS INDEXED

WEB OF SCIENCE™

Selection of our books indexed in the Book Citation Index
in Web of Science™ Core Collection (BKCI)

Interested in publishing with us?
Contact book.department@intechopen.com

Numbers displayed above are based on latest data collected.
For more information visit www.intechopen.com

Flexible Ferroelectric BaTiO$_3$ – PVDF Nanocomposites

V. Corral-Flores and D. Bueno-Baqués
Research Center for Applied Chemistry,
Mexico

1. Introduction

Ferroelectric materials are considered as smart materials, since they can be configured to store, release or interconvert electrical and mechanical energy in a well-controlled manner. Their exceptionally large piezoelectric compliances, pyroelectric coefficients, dielectric susceptibilities and electro-optic properties make them very attractive for nanotechnology-related applications such as high energy density capacitors, pyroelectric thermal imaging devices, gate insulators in transistors, electro-optic light valves, thin-film memory elements, multiferroic transducers, energy harvesters, etc. (Alpay et al., 2009, Nonnenmann & Spanier, 2009; Scott, 2007; Leionen et al., 2009)

The most common ferroelectric materials in commercial applications are ceramics, such as lead zirconate-titanate (PZT), barium titanate (BTO), calcium-copper titanate CaCu$_3$Ti$_4$O$_{12}$ (CCTO), sodium niobate (NaNbO$_3$), among others, which present a high dielectric constant, high dipole moment and high electromechanical coupling coefficient. Ferroelectric ceramics have been recently synthesized by solvothermal (Wada et al., 2009), coprecipitation (Hu, et al., 2000), sol-gel (Kobayashi et al., 2004), and template assisted methods (Rorvik et al., 2009), in order to obtain nanostructured materials. Considering the toxicity of lead and its compounds, there is a general awareness for the development of environmental friendly lead-free materials (Panda, 2009; Jia et al., 2009). In the development of this work, we have chosen BTO for its excellent ferro-, piezo-, and di-electric properties.

Barium titanate presents the perovskite crystal structure, which has the general formula $A^{2+}B^{4+}O_3^{2-}$, where A represents a divalent metal ion (barium) and B represents tetravalent metal ions (titanium in this case). Above the Curie temperature (T$_C$), the crystal has a cubic symmetry, a centrosymmetric microstructure where the positive and negative charges coincide. Below T$_C$, crystals have a tetragonal symmetry. This form has no center of symmetry, in each unit cell exhibits an electric dipole that can be reoriented by an applied electric field. The material is then called ferroelectric.

Ceramics, however, are brittle and require high temperature processing. By the other side, ferroelectric polymers present good mechanical properties, can be formed in complex shapes at low temperature, are flexible and have high dielectric strengths; although the ferroelectric properties and dielectric constant are lower than ceramics. Poly(vinylidene fluoride) (PVDF) is an electroactive polymer that exhibits polymorphism. Its most common crystalline phases are: α, β, γ and δ phases; also known as form II, I, III and IV respectively.

Each form has its own characteristic unit cell due to chain conformation. α phase crystallizes in an orthorhombic cell, where two chains are opposite packed canceling the individual dipole moments. The chain conformation consists of alternating trans and gauche sequences. In β phase, two chains in all-trans planar zigzag conformation are packed into an orthorhombic unit cell. The fluorine atoms are positioned on one-side of the unit cell resulting in a net dipole moment of 2.1 debye, the highest among all phases. In γ phase, two opposite chains conform a monoclinic crystal lattice, where only a fraction of dipole moments are cancelled. δ phase is formed when α phase is electrically poled, and one of the chains align parallel to the other, resulting in a weak net dipole moment. The crystal lattice parameters are identical to α phase (Schwartz, 2002).

A hybrid ceramic-polymeric composite is a convenient solution to tune both mechanical and electrical properties. In this respect, several systems have been already developed, such as CCTO - poly(vinylidene fluoride – trifluoroethylene) [P(VDF-TrFE)] (Arbatti et al., 2005), BTO – PVDF (Chanmal & Jog, 2008), MWCNTs – BTO – PVDF (Dang et al., 2003), Sm/Mn doped $PbTiO_3$ - epoxy (Li et al., 2003), and PZT – Rubber (Qi et al., 2010). Composites are complex, heterogeneous and usually anisotropic systems. Its properties are affected by many variables, including constituent material properties, geometry, volumetric fraction, interface properties, coupling properties between the phases, porosity, etc. Connectivities between the phases play a very important role in the ultimate properties of the composites. The connectivity has great importance in a multiphase material because it heavily influences the mechanical, electrical and thermal fluxes between the phases. From matrix-loaded composites to highly sophisticated arrangements, composites can be designed to tailor the acoustic impedance, coupling constant and mechanical quality factor, as compared to bulk ceramics.

In nanotechnology applications, ferroelectric ceramics have to overcome some size scaling challenges, since their main properties can be dramatically affected when the grain size decreases to a certain limit, where the material suffers either changes in Tc, phase transition or variations in its polarization state (Eliseev & Morozovska, 2009). In a similar manner, ferroelectric polymers have to be processed in a way that enhances its crystalinity and favours the growing of the polar phase. These two issues must be carefully addressed when processing hybrid ceramic-polymeric composites.

Electrospinning is a versatile technique widely used to produce either polymer (An et al., 2006; Koombhongse et al., 2001) or ceramic nanofibers (Lu et al., 2006; Azad, 2006). Even nanocomposites have been produced by this technique (Saeed et al., 2006; Wang et al., 2004). The major components are a high voltage power supply, a container with a metallic tip to feed the polymer solution and a grounded collector. Electrospinning occurs when the electrical forces at the surface of a charged polymer solution droplet overcome the surface tension. The solution is ejected as an electrically charged jet towards the oppositely charged electrode, while the solvent evaporates, leading to the formation of dry nanofibers. When the jet flow away from the droplet to the target, it undergoes a series of electrically driven bending instabilities, following a complex path that gives rise to a series of looping and spiraling motions. The jet elongates, and this stretching significantly reduces its diameter (Reneker et al., 2000). Since this technique involves high electric fields, it is then expected to enhance the formation of polar phases in polymorph polymers, such as PVDF (Ramakrishna et al., 2010).

Template-assisted synthesis is a simple method to produce one-dimensional nanostructures and nanotube arrays. The templates, such as porous anodic alumina, have pores in which a

solution containing the desired components can be incorporated, forming the nanotubes after solvent evaporation (Rorvik et al., 2009).

This chapter covers several configurations and connectivities of hybrid barium titanate - poly(vinylidene fluoride) (BTO – PVDF) nanocomposites and nanostructures:

i.   BTO nanoparticles embedded in a PVDF matrix.
ii.   BTO nanoparticles embedded in PVDF nanofibers.
iii. BTO nanofibrous membranes in a PVDF matrix.
iv.   BTO – PVDF nanotube arrays.

Dielectric properties and polarization hysteresis are presented and discussed. This study is expected to further expand the understanding and range of applicability of these functional nanostructured materials.

2. Experimental

The ceramic nanoparticles were obtained by microwave assisted hydrothermal method, while the nanofibrous membranes were synthesized by electrospinning technique. PVDF (Kynar 761 kindly supplied by Arkema) was processed by spin-coating and electrospinning to obtain films and nanofibers, respectively. BTO – PVDF nanotube arrays were prepared by template assisted synthesis, combining sol-gel and sol-humectation in a porous membrane. All chemicals used in this study were reagent grade purchased from Sigma-Aldrich.

2.1 BTO nanoparticles embedded in a PVDF matrix

BTO nanoparticles were synthesized in two steps procedure. First, TiO_2 nanoparticles were obtained by direct precipitation from a $TiCl_4$ solution in ice-cold water after seven days of reaction. Second, TiO_2 nanoparticles were subjected to microwave-assisted hydrothermal conditions in a CEM oven model MARS 5. A barium hydroxide aqueous solution under a Ti:Ba molar ratio of 1:1.8 was used as the reaction media; the hydrothermal reaction took place at 150°C for 15 min. After washing, the nanoparticles were capped with 3-aminopropyl triethoxysilane at acidic media (acetic acid was added until a pH of 4 was reached) under microwave-assisted hydrothermal conditions at 150°C for 60 min. Samples at this stage were named as BTO-MWHT.

BTO-PVDF films were obtained by spin-coating PVDF-N,N-dimethylformamide (DMF) solutions containing silane-capped BTO nanoparticles at the following BTO:PVDF weight ratios: 1:10, 1:20 and 1:100. PVDF concentration in DMF was kept at 12 wt.% for the suspensions with high content of BTO, and 14 wt.% for the 1:100 ratio. Samples after this procedure were named as BTO-MWHT-PVDF-SC.

2.2 BTO nanoparticles embedded in PVDF nanofibers

BTO-PVDF suspensions (as described in 2.1) were electrospun at 15 kV and 20μA in a horizontal set-up. The feeding rate was 0.5 ml/hr and the tip-to-collector distance was varied from 10 to 15 cm. Electrospun samples were named as BTO-PVDF-ES.

2.3 BTO nanofibrous membranes embedded in a PVDF matrix

BTO nanofibrous membranes were obtained by electrospinning a 1 M precursor solution containing the corresponding metal ions. Titanium butoxide and barium acetate at a 1:1 molar ratio were dissolved in methoxyethanol and acetic acid. Poly(vinyl pirrolidone) was

added to facilitate the electrospinning process. The following conditions were used: feed rate of 0.5 ml/hr, 15 kV and tip-to-collector distance in the range of 10 to 15 cm. The electrospun nanofibrous membranes were sintered at 800°C for 2 hours to obtain the ceramic phase. Then the BTO nanofibrous membranes (named as BTO-ES) were embedded in a PVDF matrix by spin-coating a 15 wt.% PVDF solution over the membranes in a conductive Pt-Si substrate. After deposition, samples were heat-treated at 60°C for 1 hour to crystallize the beta phase of the polymer. The nomenclature for these samples was set as BTO-ES-PVDF-SC.

2.4 BTO – PVDF nanotube arrays

These arrays were obtained in two steps: synthesis of BTO nanotubes and wetting of the nanotubes in a PVDF solution. To synthesize the BTO nanotubes, alumina templates (Whatman Anodisc 13) were immersed in the precursor solution described in 2.3, and then the excess solution was wiped off. In order to crystallize the BTO ceramic phase, the samples were heat treated at 400°C for 1 hr and then at 700°C for 2 hours under a heating and cooling rate of 2°C/min. To obtain the PVDF nanotubes, the templates containing BTO nanotubes were immersed in a 5wt.% PVDF-DMF solution, then the solvent was evaporated at room temperature. This set of samples was named as BTO-PVDF-NT.

3. Results

Crystalline phases were determined by X-ray diffraction (XRD, Siemmens D-5000), morphology was studied by scanning and transmission electron microscopy (SEM, Jeol JSM-740IF and TEM, Fei Titan 80), and infrared spectroscopy (FTIR, IR-Nexus 470) -using a micro-ATR (attenuated total reflectance) accessory- was used to determine the fraction of beta phase in the polymer.

Polarization hysteresis loops were measured with a 300 Hz driving signal amplified by a TEGAM HV. Sample response was collected with virtual ground charge/current amplifier. Field and current signals were digitized simultaneously and numerically processed to obtain the electric displacement and polarization. The dielectric properties were measured using a TEGAM 3550 impedance analyzer in a range from 100 Hz to 5 MHz.

3.1 Structural characterization

X-ray diffraction patterns are shown in Fig. 1. The tetragonal doublet corresponding to (002) and (200) in BTO was not clear at the test conditions, probably due to the peak widening, or a mixture of cubic and tetragonal phases. However, a pattern refinement (using the program PowderCell 2.4) revealed that the best fit is obtained from the tetragonal reference. The Miller indexes for tetragonal barium titanate are presented in Fig. 1. The crystallite size and cell parameters obtained from the refinement are presented in Table 1. According to these results, all samples presented small crystallite size in the range of 20 – 26 nm.

BTO surface functionalization with silane at hydrothermal conditions altered both the crystallite size and the degree of tetragonality, possibly due to the acidic conditions and the extended reaction time. Additionally, the small diffraction peaks present in this sample (Fig. 1) were identified as TiO_2, both rutile and anatase phases, which presumably were formed by the dissolution of BTO and subsequent leaching of barium during the functionalization reaction. Nevertheless, the surface functionalization of the nanoparticles was crucial for its proper dispersion in the PVDF matrix. A micrograph showing the BTO-MWHT-Silane

nanoparticles is presented in Fig. 2. Average particle size was determined as 31.6 nm, slightly higher than the crystallite size estimated from XRD results. This difference can be attributed to the silane layer, and/or the possible presence of an amorphous (distorted) phase at the surface of the nanoparticles.
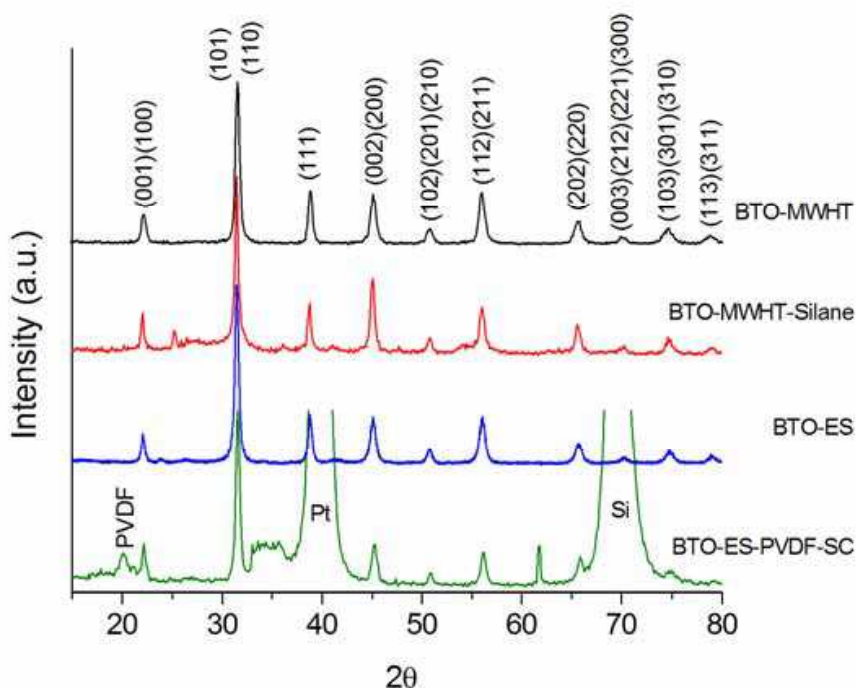

Fig. 1. X-ray diffraction of BTO samples obtained from different techniques.

Sample	d(nm)	a (Å)	c(Å)	DoT	Rp(%)
BTO-MWHT	20	4.0176	4.0458	1.00702	9.72
BTO-MWHT-Silane	24	4.0182	4.0192	1.00025	13.45
BTO-ES	23	4.0039	4.0317	1.00694	10.90

Table 1. Refinement results: crystallite size (d), cell parameters (a and c), profile R factor (Rp) and the degree of tetragonality (DoT) for BTO tetragonal phase.

Electrospun BTO nanofibers showed a single phase XRD pattern, very similar to that of the BTO nanoparticles (Fig. 1), however, its morphology is clearly different. Figure 3 shows BTO nanofibers obtained at 15 kV and tip-to-collector distance of 15 cm, before and after heat treatment. As-spun fibers are long and smooth, with average diameter of 110.4 ±48.2, ranging from 27 to 362 nm. Sintered nanofibers preserved its morphology while presenting a rough surface, revealing the presence of grains. These nanofibers presented a reduction in size, with an average diameter of 105.5 ±16.5 nm, ranging from 51 to 225 nm. Apparently, the thinnest nanofibers are fractured and lost during heat treatment.

When BTO nanofibrous membranes were immersed in PVDF to obtain hybrid ceramic-polimeric composites, the nanofibers were not modified in terms of morphology or crystallograpy. XRD (Fig. 1) showed the presence of silicon and platinum from the substrate, together with some other unknown reflections that are attributed also to the substrate. PVDF was confirmed from the peak at around 20.1 degrees in 2θ. According to several

reports, α phase can be identified by diffraction peaks present at 17.83, 18.52, 20.1 and 25.88°, β phase at 20.44° and γ phase at 26.74° (Nasir et al., 2007; Esterly & Love, 2004; Gao et al., 2006). However, it was difficult to distinguish between alfa and beta phases. For this purpose, infrared spectroscopy was used.
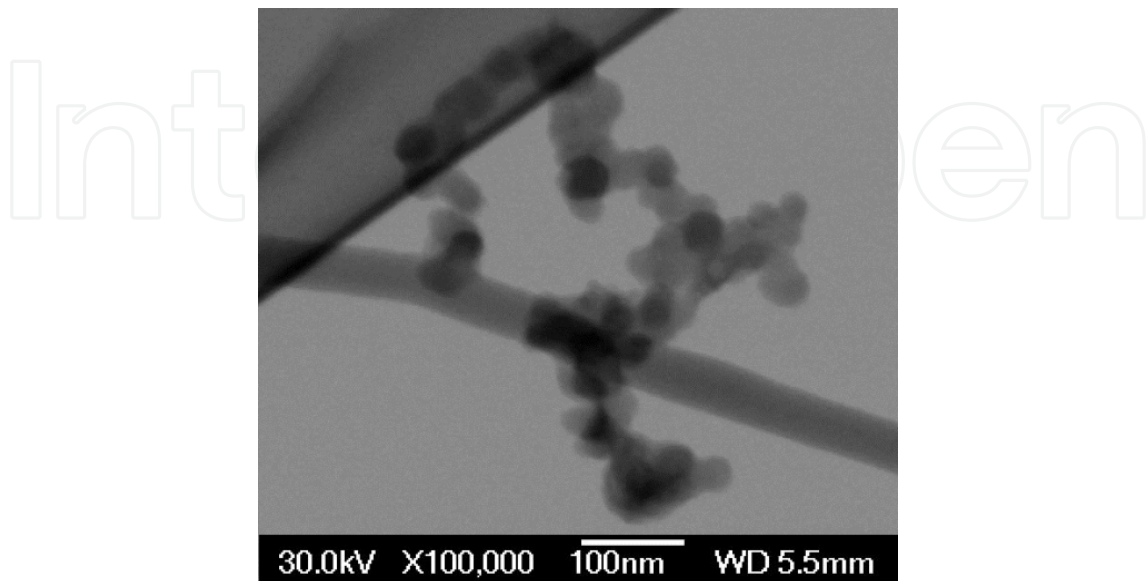

Fig. 2. STEM Micrograph of the BTO nanoparticles obtained by microwave-assisted hydrothermal method and capped with silane (sample BTO-MWHT-Silane).
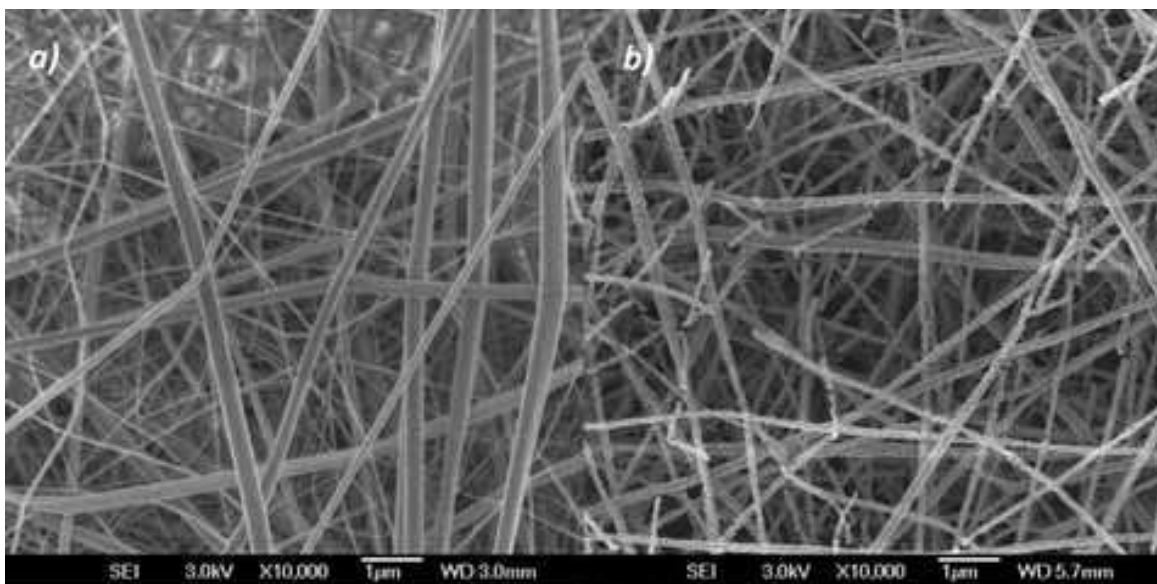

Fig. 3. SEM micrographs of BTO nanofibers, collected at 15 kV and 15 cm between electrodes, (a) before heat treatment and (b) sintered at 800°C.

FTIR spectra are shown in Figure 4. The absorption bands corresponding to the crystalline phases are shown by dotted lines for clarity. Absorption bands at 762, 795 and 974 cm^{-1} correspond to α phase, bands at 839 and 1276 cm^{-1} are assigned to β phase, while γ phase is identified by the band at 1235 cm^{-1} (Yee et al., 2007). PVDF raw material showed predominantly alfa phase. Samples obtained either from electrospinning or spin-coating

showed a substantial reduction on the content of this non-polar phase, while the presence of beta phase was enhanced in some cases.
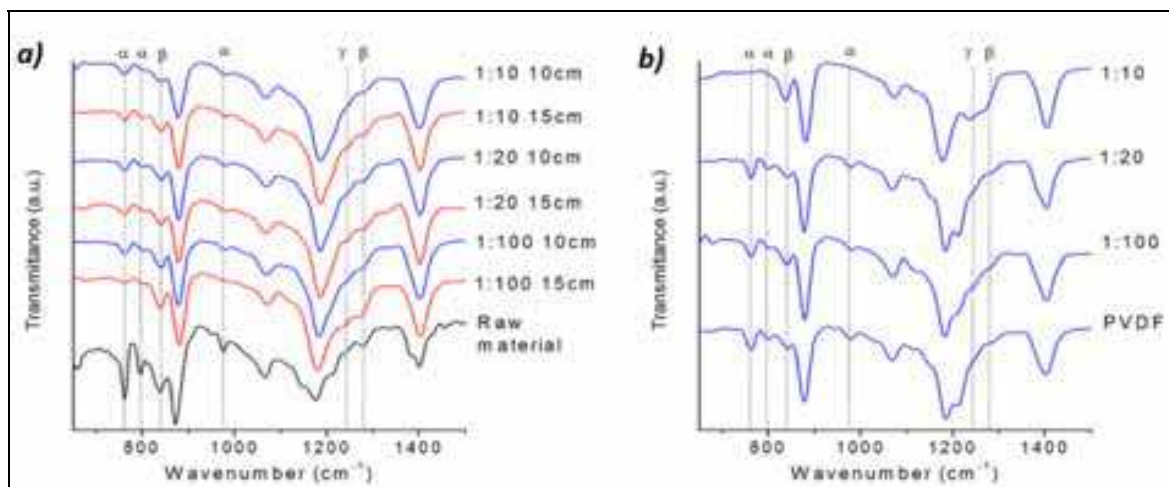

Fig. 4. FTIR-ATR spectra of BTO-PVDF samples obtained from (a) electrospinning technique and (b) spin-coating.

The fraction of beta phase was estimated from the equation proposed by Gregorio & Cestari (Gregorio & Cestari, 1994) and later used by several authors (Salimi & Youse, 2004; Jiang et al., 2007; Sobhani et al., 2007; Andrew & Clarke, 2008):

$$F(\beta) = \frac{A_\beta}{1.26 A_\alpha + A_\beta} \tag{1}$$

Where A_a and A_β are the absorption band intensity for α and β phases, respectively. The fraction of beta phase of the samples containing PVDF in the present study is shown in Table 2. PVDF raw material presented a fraction of beta phase of 0.12. Samples obtained from electrospinning technique showed higher beta content than that of those from spin-coating. This could be attributed to differences in the methods, such as the solvent evaporation rate and the presence of the electric field during electrospinning.

BTO:PVDF ratio	Technique	Distance (cm)	Beta fraction
0:1	ES	10	0.69
0:1	ES	15	0.66
0:1	SC	-	0.38
1:10	ES	10	0.60
1:10	ES	15	0.65
1:10	SC	-	1.00
1:20	ES	10	0.63
1:20	ES	15	0.64
1:20	SC	-	0.46
1:100	ES	10	0.60
1:100	ES	15	0.86
1:100	SC	-	0.47

Table 2. Beta fraction of electrospun (ES) and spin-coated (SC) samples. Distance stands for the tip-to-collector distance in electrospinning set up.
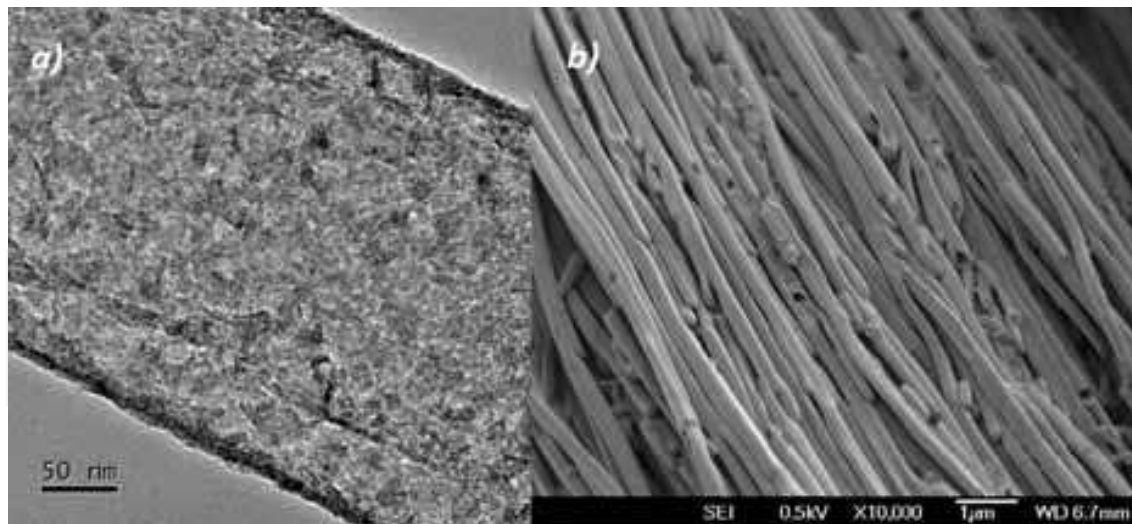
Fig. 5. Micrographs of (a) a BTO nanotube and (b) PVDF nanotubes, both obtained in an alumina template with porous diameter of 200 nm.

In order to release the nanotubes from the alumina template nanotube arrays, the template was dissolved in a 5M NaOH solution. TEM revealed the formation of ceramic BTO nanotubes with average wall thickness of 11 nm (as shown in Fig. 5a). The ceramic nanotubes were crystalline in nature and presented small crystallites in the order of 4 to 5 nm. PVDF nanotubes, observed by SEM (Fig. 5b), reproduced the inner morphology of the alumina templates, even small defects. The average diameter was consistent with that of the templates, and the length was expected to reach the template thickness (60 microns).

3.2 Electric behavior
Samples were clamped between highly smooth parallel contact plates cut from an Ir-Pt coated silicon wafer for electric polarization measurements, while Au-Pd was deposited as top electrode before acquiring the dielectric properties. The electric behaviour is discussed below.

3.2.1 Electric polarization
Electric polarization of electrospun samples (BTO-PVDF-ES) revealed a linear behaviour in most of the cases, due to the porosity inherent to the fibrous array. An estimate of the effective area in contact with the top electrode is 60%, being the rest essentially air. Samples containing a BTO:PVDF ratio of 1:10 presented a non-linear behaviour, especially when electrospun at a distance of 15 cm (Fig. 6). These results characterize a lossy ferroelectric material (Scott et al., 1998), and are in agreement with the fraction of beta phase calculated from FTIR spectra (Table 2) which is higher for the sample obtained at 15 cm. It is known that the electrospinning conditions such as the tip-to-collector distance and applied voltage play an important role in the morphology and size of the fibers (Azad, 2006), and additionally, can affect the crystallization of polar phases in the case of ferroelectric polymers (Yee et al., 2007).

A similar response was obtained from electrospun BTO fibers (sample BTO-ES), as shown in Fig. 7, due to the low density of the sample and the contribution of air in the measurement. However, the concave region in the graph is indicative of the ferroelectric properties of BTO. Addition of PVDF to the BTO fibers (sample BTO-ES-PVDF-SC) did not change this behaviour, note that the later sample was measured at a lower applied voltage.
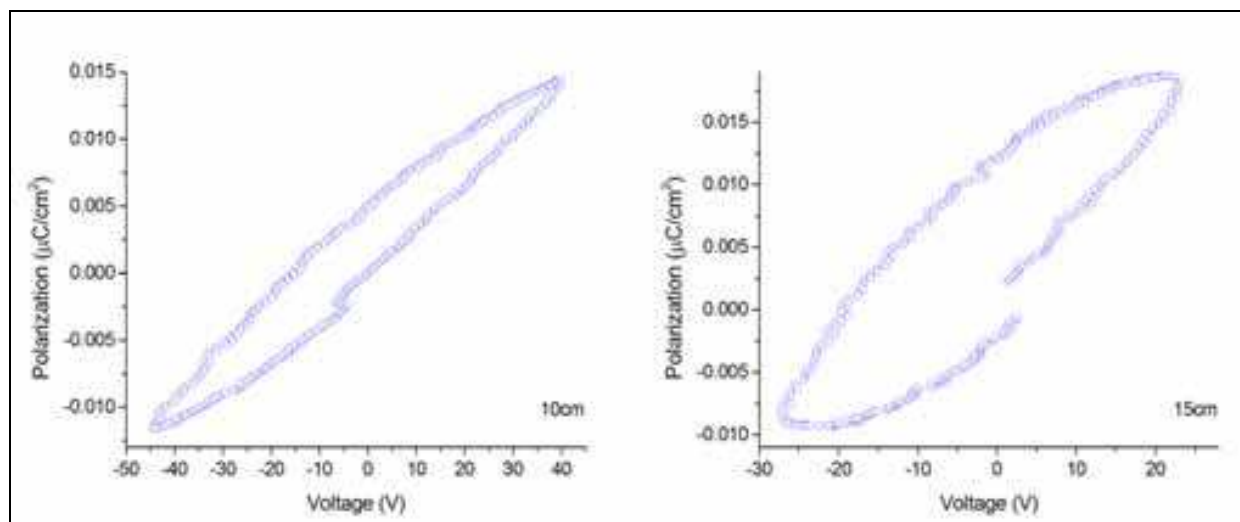
Fig. 6. Electric polarization of the electrospun samples with a BTO:PVDF ratio of 1:10. Tip-to-collector distance was 10 and 15 cm.
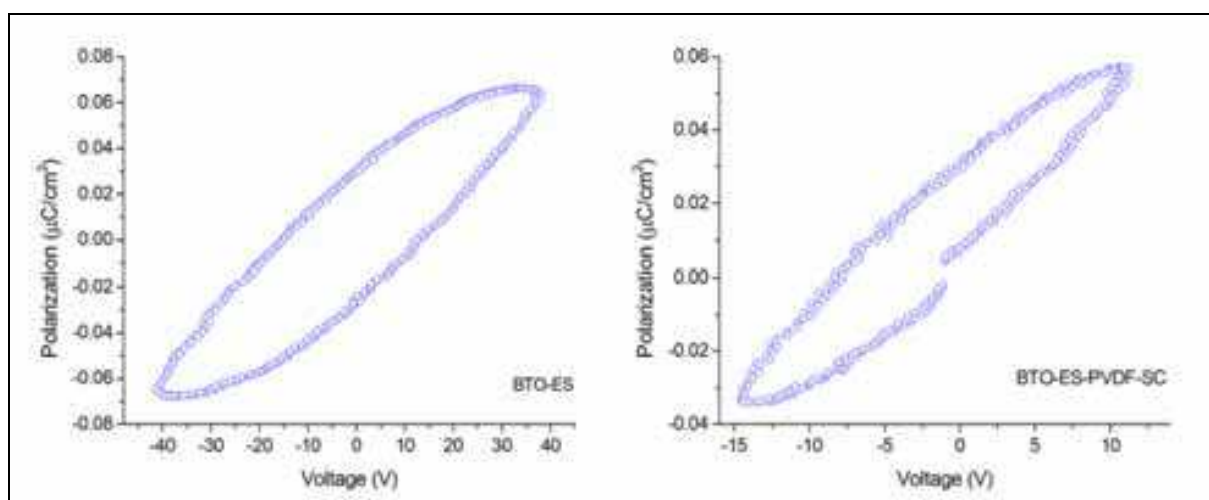

Fig. 7. Electric polarization of electrospun BTO and electrospun BTO with PVDF deposited by spin-coating.

Films of PVDF with BTO nanoparticles (samples BTO-MWHT-PVDF-SC), prepared by spin-coating, exhibited a ferroelectric response based on the amount of nanoparticles present. As shown in Fig. 8, the sample with the highest content of BTO nanoparticles (1:10 ratio) showed a nice ferroelectric hysteresis loop that reflects that in fact, the composition, geometry and connectivity of this sample are optimum to enhance the ferroelectricity of hybrid ceramic-polymeric composites.

In an opposite behaviour to the system BTO-MWHT-PVDF-SC, the nanotube arrays showed a better ferroelectric response when only the polymer was present. As shown in Fig. 9, the PVDF nanotube array (PVDF-NT) is ferroelectric, despite that the alumina template is a dielectric. The electric polarization was calculated taking into account the total area of the alumina templates (13 mm), however, the effective area in contact with the top electrode is much lower, estimated from SEM micrographs as 66% of the total template area.
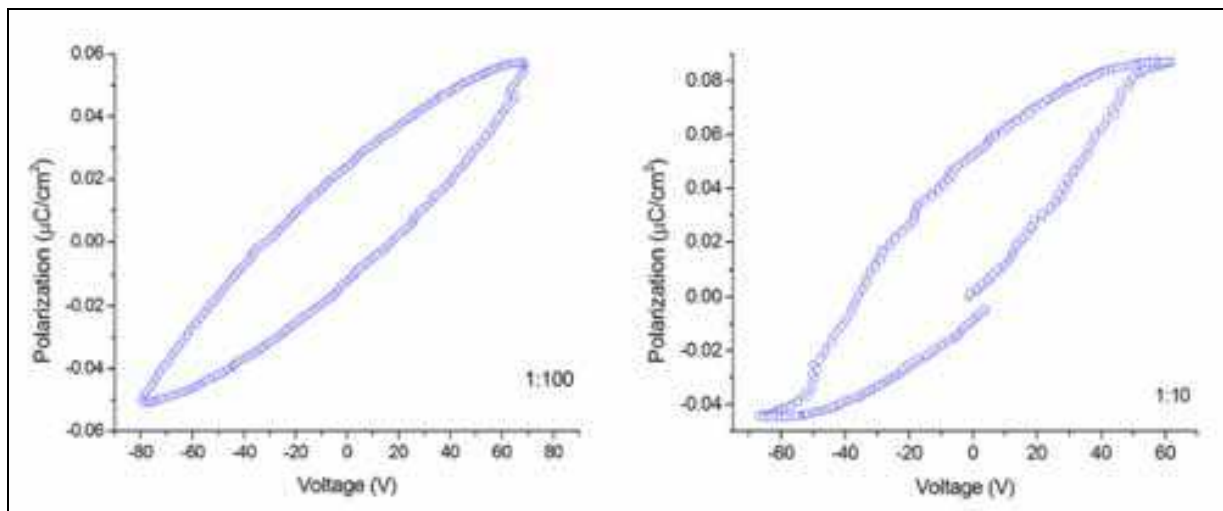
Fig. 8. Electric polarization of BTO-PVDF films deposited by spin-coating. BTO:PVDF weight ratio is presented.
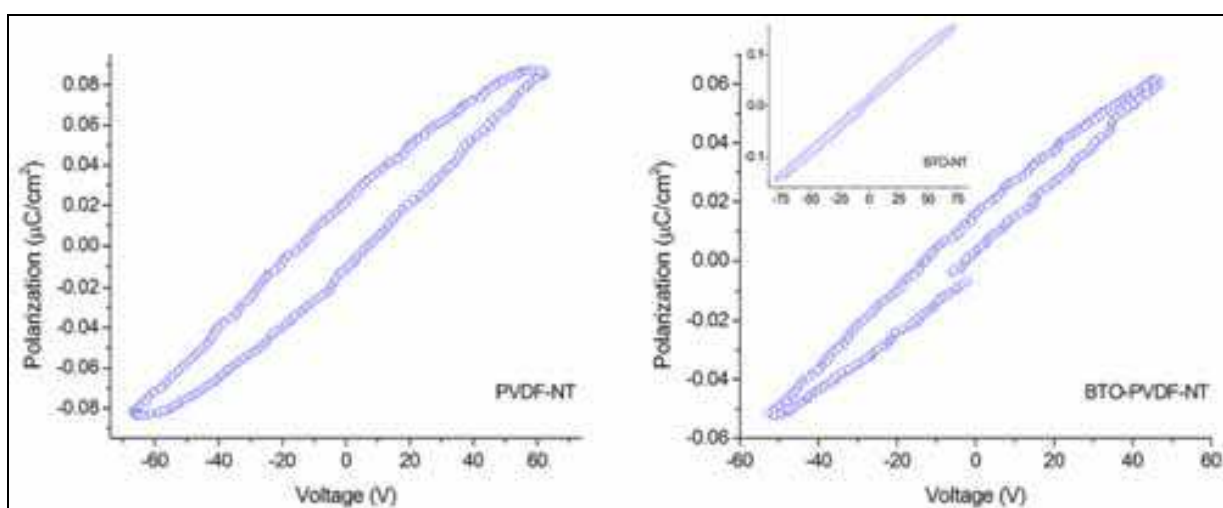

Fig. 9. Electric polarization of BTO-PVDF nanotube arrays. The response of the pure BTO nanotubes is presented as inset.

3.2.2 Dielectric spectroscopy and impedance analysis

Figure 10 shows the dielectric permittivity and loss of single phase and composite nanotube arrays measured at room temperature from 100 Hz to 3 MHz.

As observed, the dielectric permittivity decreases with the addition of PDVF layer on top of the BTO nanotube structure formed in the template. This could be related to the complex geometry of the composite structure, in which PVDF layer is encapsulating the BTO and alumina template. It is known (Tsangaris 1999 as cited in Patsidis & Psarras 2008) that Maxwell-Wagner-Sillas effect heavily influences the electrical behaviour of systems with complex electrical heterogeneities, where large accumulation of charges can take place at the interface of the system. In present composites, based on the fact that dielectric permittivity of BTO is considerable higher than alumina, large unbounded charges can arise from the ceramics interface. The arising limitation of field induced dipoles to follow the alternation of

the electric field will shift the associated relaxation process to lower frequencies, as suggested by the behaviour of the dielectric loss in the case of the BTO-NT sample.   With the addition of PVDF layer, competing phenomena could arise from trapped charges at the BTO – PVDF interface, leading to self balance stable state with a consequent change in the relaxation behaviour.
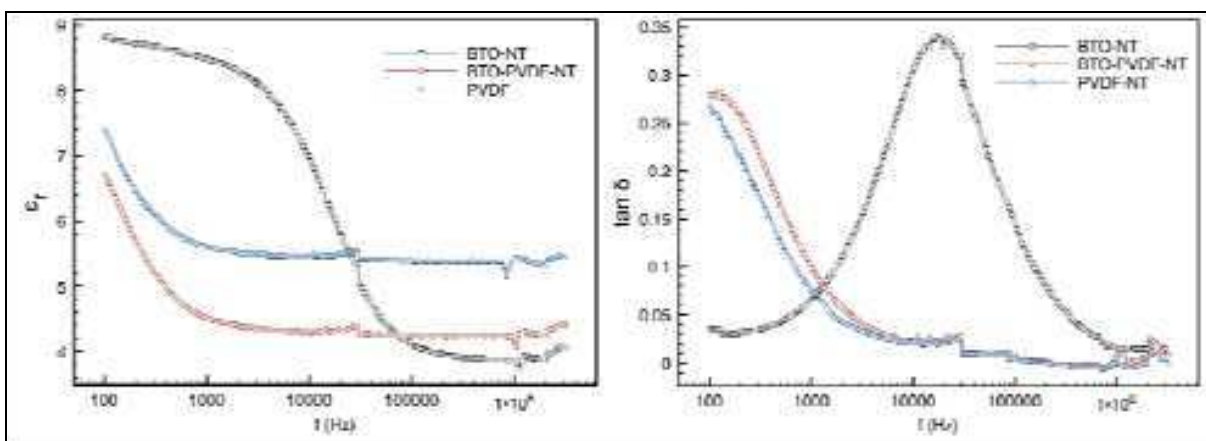

Fig. 10. Dielectric permittivity and dielectric loss of the nanotube arrays.

The real and imaginary impedance components increase with the inclusion of PDVF nanotubes at low frequencies, as shown in figure 11. This could indicate a better insulation at low frequencies introduced by the PVDF layer. At high frequencies the AC conductivity increases.
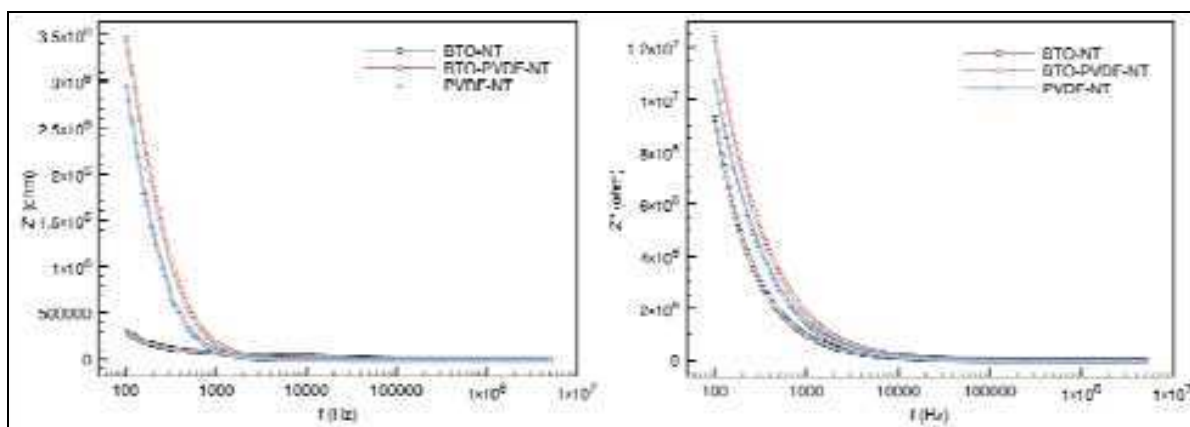
Fig. 11. Real and imaginary impedance components of the nanotube arrays.

Figure 12 shows the dielectric permittivity and dielectric loss of the BTO-MWHT-PVDF-SC film composites. As shown, dielectric permittivity increases with the increase in the ceramic loading and could be attributed to an enhanced polarization from dipole-dipole interactions in more closely aggregated nanocrystallites of the ceramic phase. Also, dielectric permittivity decreases for higher frequencies values, more rapidly for frequencies above 100 kHz. Several unset are observed for both compositions, which can be related to the dipole orientation polarization of the BaTiO$_3$ nanoparticles. Dielectric loss shows one noticeable relaxation at frequency close to 3 Hz for both composite samples. Due to the almost similar frequency values and shape it is suggested that this relaxation should be related to the

polymer phase. This can be associated to cooperative motions in the main polymer chains related to the non-polar α phase in the PVDF. Several authors have discussed and proposed different mechanisms for this phenomenon (Kochervinskii, 2007 as cited in Chanmal & Jog, 2008).
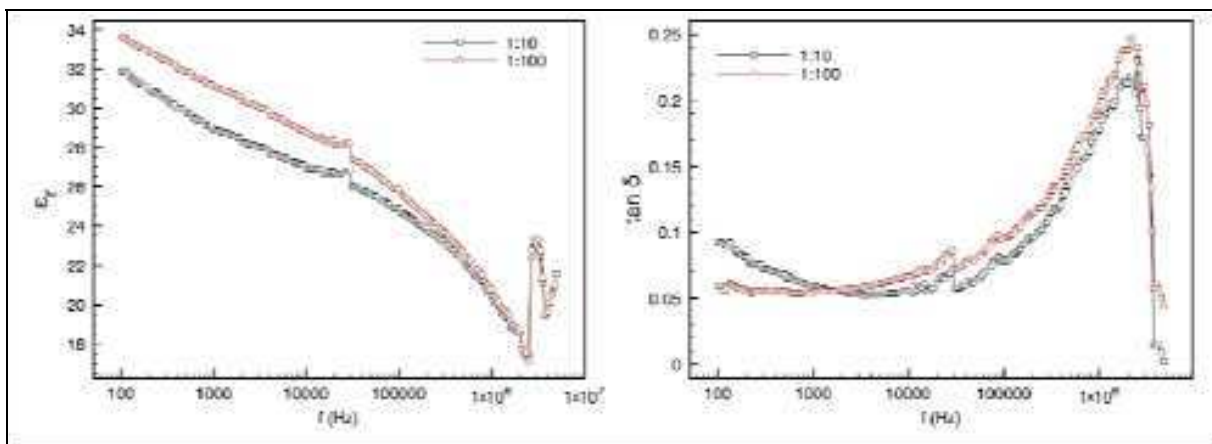

Fig. 12. Dielectric permittivity and dielectric loss for BTO-MWHT-PVDF-SC film composites

Real and imaginary parts of the impedance for the BTO-MWHT-PVDF-SC film composites are shown in figure 13. As can be observed in the figures, both impedance components are respectively very similar to that for the films with different BTO content. Also, real (Z') and imaginary (Z'') components decrease with the increase in frequency. The behaviour of Z' indicates an increase in the AC conductivity of the material, while Z'' suggest a Debye type relaxation process in the samples. The fact that both curves merge above 10 kHz could imply that dipole polarization in the BTO particles and trapped charges on their surfaces predominates over the space charge effects.
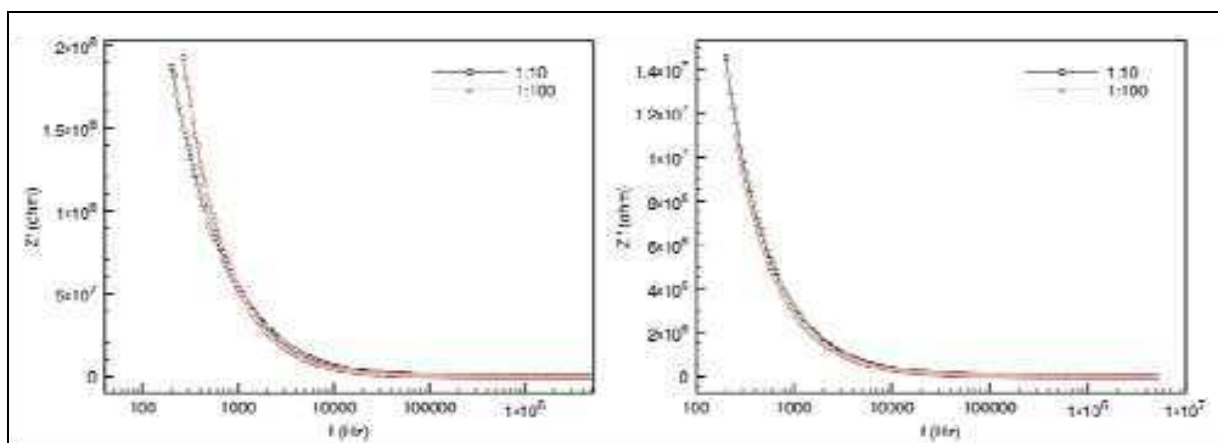

Fig. 13. Real and imaginary parts of the impedance for BTO-MWHT-PVDF-SC film composites as a function of frequency.

4. Conclusion

Barium titanate – Poly(vinylidene fluoride) hybrid composites with different morphologies were synthesized by combining several appropriate techniques: microwave-assisted

hydrothermal, electrospinning, spin-coating, precipitation and sol-humectation. Different connectivities were obtained by the use of BTO nanoparticles and nanofibers in PVDF films and nanofibers. We demonstrated the suitability of such techniques to synthesize hybrid ceramic-polymeric ferroelectric nanocomposites. BTO crystallite size was 20 and 24 nm, when synthesized by microwave-assited hydrothermal method and electrospinning technique, respectively. Single tetragonal phase was obtained in both cases, with a degree of tetragonality or around 1.007. A silane functionalization by MWHT resulted in a slight growth of BTO nanoparticles accompanied by a partial dissolution, leading to the formation of secondary phases. Additionally, a decrease in the degree of tetragonality was detected. The fraction of beta phase present in the polymer was higher than the raw material, as revealed by FTIR analysis. Samples obtained by electrospinning technique presented, in general, higher content of beta phase than those obtained by spin-coating.

Electrospun samples of the system BTO-PVDF-ES presented an electric behaviour from linear dielectric to lossy ferroelectric when the amount of BTO nanoparticles increased. Sample with a BTO:PVDF weight ratio of 1:10 showed a good ferroelectric-like response when electrospun at a tip-to-collector distance of 15 cm. Similarly, electrospun BTO ceramic nanofibers showed a ferroelectric response, as well as the sample BTO-ES-PVDF-SC.

Films of the system BTO-MWHT-PVDF-SC showed the best ferroelectric results of all series. The sample with BTO:PVDF weight ratio of 1:10 showed a hysteresis loop indicative of ferroelectric properties. In contrast, nanotube arrays presented an opposite behaviour, since PVDF nanotube array presented a better response than hybrid PVDF-BTO and even BTO-NT.

Dielectric spectroscopy reveals a complex polarization and relaxation behaviour in the composites. Depending on the geometry and connectivity of the phases competing phenomena related to the charge accumulation at the interfaces and trapped charges at the surface of the ceramic phase takes place. However it is suggested that with the increase of the polymer content, the later mechanism prevails.

5. Acknowledgment

6. References

Alpay, S. P., Nagarajan, V. & Rossetti, G. A. Jr. (2009) Recent developments in ferroelectric nanostructures and multilayers, J. Mater. Sci. Vol. 44, pp. (5021–5024)

An, H., Shin C. & Chase, G.G. (2006). Ion exchanger using electrospun polystyrene nanofibers. *J. of Membrane Science,* Vol. 283, (2006), pp. (84-87)

Andrew, S. & Clarke, D.R. Effect of electrospinning on the ferroelectric phase content of polyvinylidene difluoride fibers, *Langmuir*, Vol. 24 (2008) pp. (670-672)

Arbatti, M., Shan, X. & Cheng, Z. Y. (2005) New High-Dielectric-Constant Polymer-Ceramic Composites, *Mater. Res. Soc. Symp. Proc.,* Vol. 847

Azad, A.M. Fabrication of yttria-stabilized zirconia nanofibers by electrospinning. *Mat. Lett.*, Vol. 60, (2006), pp. (67-72)

Chanmal, C. V. & Jog, J. P. (2008). Dielectric Relaxations in PVDF/BaTiO$_3$ Nanocomposites. *eXPRESS Polymer Letters*, Vol. 2, No. 4, (2008) pp. (294–301)

Dang, Z. M., Fan, L. Z., Shen, Y., & Nan, C. W. (2003) Dielectric behavior of Novel Three-Phase MWNTs/BaTiO3/PVDF Composites, *Mat. Sci. Eng.* Vol. B103, pp. (140-144)

Eliseev, E. A. & Morozovska, A. N. (2009) General approach for the description of size effects in ferroelectric nanosystems, *J. Mater. Sci.* Vol. 44, pp. (5149–5160)

Esterly, D.M. & Love, B.J. Phase transformation to β-poly(vinylidene fluoride) by milling. *J. Polym. Sci. B: Polym. Phys.,* Vol. 42 (2004) pp. (91-97)

Gao, K., Hu, X., Dai, C. & Yi, T. Crystal structures of electrospun PVDF membranes and its separator application for rechargeable lithium metal cells. *Mat. Sci. and Engineering B*, Vol. 131 (2006) pp. (100-105)

Gregorio, R.Jr. & Cestari, M. Effect of crystallization temperature on the crystalline phase content and morphology of poly(vinylidene fluoride), *J. Polym. Sci. B: Pol. Phys.,* Vol. 32, No. 5 (1994) pp. (859-870)

Hu, M. Z. C., Miller, G. A., Payzant, E. A. & Rawn, C. J. (2000) Homogeneous (co)precipitation of inorganic salts for synthesis of monodispersed barium titanate particles. *J. Mat. Sci.* Vol. 35, pp. (2927-2936)

Jia, Q., Shen, B., Hao, X. Song, S. & Zhai, J. (2009) Anomalous dielectric properties of Ba$_{1-x}$Ca$_x$TiO$_3$ thin films near the solubility limit, *Materials Letters*, Vol. 63, pp. (464–466)

Jiang, Y., Ye, Y., Yu, J., Wu, Z., Li, W., Xu, J. & Xie, G. Study of thermally poled and corona charged poly(vinylidene fluoride) films. *Polym. Eng. and Sci.* DOI 10.1002/pen 20817 (2007) pp. (1344-1350)

Kobayashi, Y., Nishikata, A., Tanase, T. & Konno, M. (2004) Size Effect on Crystal Structures of Barium Titanate Nanoparticles Prepared by a Sol-Gel Method. *Journal of Sol-Gel Science and Technology*, Vol. 29, pp. (49-55)

Koombhongse, S., Liu, W. & Reneker, D.H. (2001). Flat polymer ribbons and other shapes by electrospinning. *J. Polym. Sci. B: Polym. Phys.,* Vol. 39, (2001), pp. (2598-2606)

Leionen, M., Palosaari, J., Hannu, J. Juuti, J. & Jantunen, H. (2009) Piezoelectric energy harvesting for powering low power electronics. In: Paukkeri, A., Yla-Mella, J. and Pongracz, E. (eds.) Energy Research at the University of Oulu. Proceedings of the EnePro Conference, June 3rd, 2009, University of Oulu, Finland. Kalevaprint, Oulu, ISBN 978-951-42-9154-8, pp. (105-109)

Li, K., Chan, H. L. W., & Choy, C. L. (2003). Samarium and Manganese-Doped Lead Titanate Ceramic Fiber/Epoxy 1:3 Composite for High-Frequency Transducer Application. *IEEE Trans. On Ultrasonics, Ferroel. Freq. Control*, Vol. 50, No. 10, (October 2003)

Lu, X., Liu X., Zhang W., Wang, C. & Wei Y. (2006). Large-scale synthesis of tungsten oxide nanofibers by electrospinning. *J. Colloid and Interface Sci.*, Vol. 298, (2006), pp. (996-999)

Nasir, M., Matsumoto, H., Minagawa, M., Tanioka, A., Danno, T. & Horibe, H. Formation of β-phase crystalline structure of PVDF nanofibers by electrospray deposition:

additive effect of ionic fluorinated surfactant. *Polymer Journal,* Vol. 39, No. 7 (2007) pp. (670-674)

Nonnenmann, S. S. & Spanier, J. E. (2009) Ferroelectricity in chemical nanostructures: proximal probe characterization and the surface chemical environment, J. Mater. Sci. Vol 44, pp.(5205–5213)

Panda, P. K. (2009) Review: environmental friendly lead-free piezoelectric materials, *J. Mater. Sci.* Vol. 44, pp. (5049–5062)

Qi, Y., Jafferis, N. T., Lyons, K. Jr., Lee, C. M., Ahmad, H. & McAlpine, M. C. (2010) Piezoelectric Ribbons Printed onto Rubber for Flexible Energy Conversion. *Nanoletters*, Vol. 10, No. 2, pp. (524–528)

Ramakrishna, S., Jose, R., Archana, P. S., Nair, A. S., Balamurugan, R., Venugopal, J. & Teo, W. E. (2010). Science and engineering of electrospun nanofibers for advances in clean energy, water filtration, and regenerative medicine. *J. Mater. Sci.,* Vol. 45, pp. (6283–6312)

Reneker, D.H., Yarin, A.L., Fong, H. % Koombhongse, S. Bending instability of electrically charged liquid jets of polymer solutions in electrospinning. *J. Appl. Phys.*, Vol. 87, (2000) pp. (4531-4547)

Rorvik, P. M., Tadanaga, K., Tatsumiago, M., Grande, T. & Einarsrud, M. A. (2009). Template-assisted synthesis of PbTiO$_3$ nanotubes. *J. European Ceram. Soc.* Vol. 29, pp. (2575-2579)

Saeed, K., Park, S.Y., Lee, H.J., Back, J.B. & Huh, W.S. Preparation of electrospun nanofibers of carbon nanotube / polycaprolactone nanocomposite. *Polymer* Vol. 47, (2006) pp. (8019-8025)

Salimi, A. & Youse., A.A. Conformational changes and phase transformation mechanisms in PVDF solution-cast films. *J. Polym. Sci. B: Polym. Phys.*, Vol. 42 (2004) pp. (3487-3495)

Schwartz, M. (Ed.). (2002). *Encyclopedia of Smart Materials,* John Wiler and Sons, Inc., ISBN 0-471-17780-6, United States.

Scott, J.F. (2007) Applications of Modern Ferroelectrics. *Science*, Vol. 315 (16 February 2007), pp. (954-959)

Scott, J.F., Alexe, M., Zakharov, N.D., Pignolet, A., Curran, C., & Hesse, D. Nano-phase SBT-family ferroelectric memories. *Integrated Ferroelectrics,* Vol. 21 (1998) pp. (1-14)

Sobhani, H., Razavi-Nouri, M., Youse, A.A. Effect of flow history on poly(vinylidene fluoride) crystalline phase transformation. *J. Appl. Polym. Sci.* Vol. 104 (2007) pp. (89-94)

Wada, S., Nozawa, A., Ohno, M., Kakemoto, H., Tsurumi, T., Kameshima, Y. & Ohba, Y. (2009) Preparation of barium titanate nanocube particles by solvothermal method and their characterization, *J. Mater. Sci.* Vol. 44 pp. (5161–5166)

Wang, M., Singh, H., Hatton, T.A. & Rutledge, G.C. Field-responsive superparamagnetic composite nanofibers by electrospinning. *Polymer* Vol. 45 (2004) pp. (5505-5514)

Yee, W.A, Kotaki, M., Liu, Y. & Lu, X. Morphology, polymorphism behavior and molecular orientation of electrospun poly(vinylidene fluoride) fibers. *Polymer,* Vol. 48 (2007) pp. (512-521)

Patsidis, A. & Psarras, G.C. Dielectric behaviour and functionality of polymer matrix – ceramic BaTiO$_3$ composites. *eXPRESS Polymer Letters*, Vol. 2, No. 10, (2008) pp. (718–726)
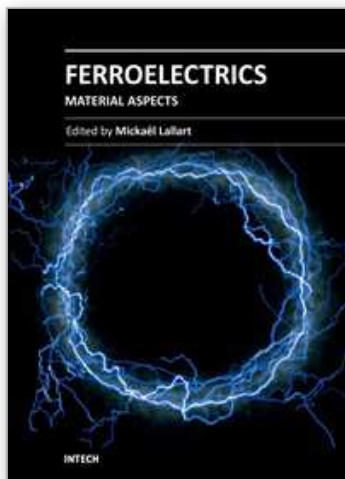
Ferroelectrics - Material Aspects

Edited by Dr. Mickaël Lallart

Ferroelectric materials have been and still are widely used in many applications, that have moved from sonar towards breakthrough technologies such as memories or optical devices. This book is a part of a four volume collection (covering material aspects, physical effects, characterization and modeling, and applications) and focuses on ways to obtain high-quality materials exhibiting large ferroelectric activity. The book covers the aspect of material synthesis and growth, doping and composites, lead-free devices, and thin film synthesis. The aim of this book is to provide an up-to-date review of recent scientific findings and recent advances in the field of ferroelectric materials, allowing a deep understanding of the material aspects of ferroelectricity.

How to reference

In order to correctly reference this scholarly work, feel free to copy and paste the following:

V. Corral-Flores and D. Bueno-Baqués (2011). Flexible Ferroelectric BaTiO3 – PVDF Nanocomposites, Ferroelectrics - Material Aspects, Dr. Mickaël Lallart (Ed.), ISBN: 978-953-307-332-3, InTech, Available from: http://www.intechopen.com/books/ferroelectrics-material-aspects/flexible-ferroelectric-batio3-pvdf-nanocomposites

INTECH
open science | open minds